Title

Determination of buried interface composition and magnetism profiles using standing-wave excited soft x-ray emission and inelastic scattering

Authors

Sell, B.C.
Ritchey, S.B.
Yang, S.-H.
et al.

Publication Date

2008-04-15

Determination of buried interface composition and magnetism profiles using standing-wave excited soft x-ray emission and inelastic scattering

B.C. Sell[1,2,§], S.-H. Yang[3], M. Watanabe[2,4],B.S. Mun[2,5], L. Plucinski[2,6], N. Mannella[1,5,7], S.B. Ritchey[1,2], A. Nambu[2,8], J. Guo[5], M.W. West[2], F. Salmassi[2], J.B. Kortright[2], S.S.P. Parkin[3], and C.S. Fadley[1,2,6]

[1]*Dept. of Physics, Univ. of California Davis, Davis, CA, 95616 USA*

[2]*Materials Sciences Division, Lawrence Berkeley National Laboratory, Berkeley, CA 94720*

[3]*IBM Almaden Research Center, San Jose, CA 95120*

[4]*RIKEN, Low Temperature Physics Lab., Hirosawa 2-1, Wako-shi, Saitama, 351-0198, Japan*

[5]*Advanced Light Source, Lawrence Berkeley National Laboratory, Berkeley, CA 94720*

[6] *Institute for Solid State Physics Research, Jülich Research Center, D-52425 Jülich, Germany*

[7]*Dept. of Applied Physics, Stanford University, Stanford CA 94305*

[8]*Dept. of Chemistry, Brookhaven National Laboratory, Upton, NY 11973*

[§]*Present address: Dept. of Physics, Otterbein College, Westerville, OH 43081*

Abstract

We demonstrate that a novel standing wave/wedge (swedge) method for probing buried solid-solid interfaces can be carried out using soft x-ray emission (XES) and resonant inelastic x-ray scattering (RIXS). For the particular case of an Al_2O_3/Fe/Cr structure of relevance to giant magnetoresistance, measurements of Fe *L* and Cr *L* total intensities and Fe *L* magnetic circular dichroism are used to derive for both the top and bottom Fe interfaces the depth profile of composition and the depth dependence of the atom-specific Fe contribution to magnetization. Using XES and RIXS in this method, as compared to photoelectron spectroscopy in prior work, permits studying more deeply buried interfaces, and suggests future applications to a wide variety of magnetic and non-magnetic nanostructures.

The increasing importance of multilayer nanostructures brings with it a need for new methods with which to study an essential structural element of them: buried layers and

buried solid-solid interfaces. Although much can be learned with existing techniques, as e.g. cross section transmission electron microscopy (perhaps with energy loss spectroscopy), and soft and hard x-ray reflectivity with variable (perhaps resonant) photon energy, it has until recently not been possible to easily apply the powerful soft x-ray techniques of photoelectron spectroscopy and x-ray emission spectroscopy selectively and non-destructively to such buried interfaces.

In the first studies of this kind, Yang, Mun and coworkers demonstrated a new method for selectively studying such buried interfaces by combining soft x-ray standing waves generated above a multilayer (ML) mirror with a wedge-profile sample configuration [1]. The sample configuration used in this method is indicated in Fig. 1. The soft x-ray incidence angle is chose to yield strong first-order Bragg reflection from the multilayer, and as a result a strong standing wave extends upward through the wedge and other layers of the actual sample on top of the multilayer. Scanning the sample in front of the small x-ray beam (along the x direction in Fig. 1) then in effect moves the fixed-phase standing wave through the different layers and interfaces of the sample, accentuating or deaccentuating different layers or interfaces in the process.

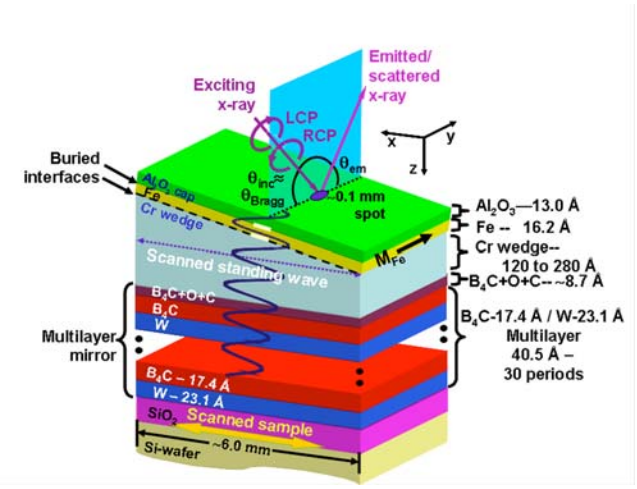

Fig. 1 – A schematic diagram of the experimental geometry used in the standing wave/wedge (swedge) method, showing the multilayer mirror that is used as a standing wave generator, on top of which has been grown a Cr wedge, an Fe layer of constant thickness, and finally a protective alumina cap. The standing wave modulation of the electric field is pinned in phase to the top of the multilayer as the position of the x-ray beam is scanned in x. Due to the wedge profile of the Cr, this scan in x also scans the standing wave through the layers and interfaces above the wedge. The Fe is magnetized in the y direction, and depth relative to the surface is defined as z. In additional rocking curve measurements, θ_{inc} is varied over the first-order Bragg angle θ_{Bragg} , with the angle between incident light and outgoing detected x-rays being fixed, in our case at 117.5°.

Standing wave-excited photoelectrons have so far been used to gain information about the compositional and magnetic structure of an Fe/Cr bilayer of relevance to giant magnetoresistance (GMR) [1], as well as the densities of states in buried layers associated with a structure related to a magnetic tunnel junction (MTJ) [2]. This standing wave/wedge (swedge) approach utilizing photoelectrons, when combined with accurate theoretical modeling including all x-ray optical effects [3], yielded concentration and magnetization profiles

with estimated accuracies of ±3 Å within the Fe/Cr bilayer. In the first study of this kind [1], the sample was grown in situ on the mirror, with Fe at a constant thickness of 16.2 Å on top of a Cr wedge varying from 100 to 300 Å in thickness. The small Fe thickness permitted probing both the Fe and the underlying Cr layer using photoelectrons. In this case, because the samples were grown *in situ,* the short inelastic mean-free paths of photoelectrons in the energy range of 500-1000 eV used (approximately 10-20 Å) was acceptable, but for many other cases of direct interest for practical devices, it is desirable to add a protective capping layer on the sample to permit transport from the synthesis system to the spectroscopy chamber. Such a capping layer would strongly attenuate the photoemission from the underlying layers of interest. By contrast, soft x-rays in the same energy range have attenuation lengths that are from one to two orders of magnitude higher for resonant or non-resonant excitation, respectively, and so should allow the study of a broader range of samples.

In this paper, we report the first demonstration of buried interface characterization via soft x-ray emission (XES) and resonant inelastic scattering (RIXS) using the swedge method. Again, we study the Fe/Cr interface, but now capped with an alumina layer to protect against degradation of the sample. This allowed the sample to be grown *ex situ*. Initial characterization was done with x-ray absorption spectroscopy (XAS) in order to determine magnetization characteristics, as well as the location of absorption edges in order to conduct RIXS measurements. Our XAS results in the Fe 2p region are shown in Fig. 2, and the form of the spectra indicate that the Fe layer had not been strongly influenced by oxidation through the protective cap [4], although the weak high-energy shoulders indicate some oxide formation, as might be expected due to interdiffusion at the Fe/Al_2O_3 interface during initial synthesis, as described below. Further characterization was done by measuring non-resonant x-ray emission spectroscopy (XES) and RIXS spectra. Utilizing circularly polarized synchrotron radiation for excitation permitted studying the Fe magnetization profile through the top and bottom interfaces of the Fe layer, something which is not possible with photoelectrons, which are primarily sensitive to the top interface due to their short inelastic mean free paths (IMFPs). Results were then compared to x-ray optical (XRO) calculations using a computer code written by Yang [3] in order to quantitatively derive the interface properties.

The schematic structure of the sample studied is depicted in Fig. 1. The sample substrate was a multilayer mirror consisting of 30 alternating B_4C-17.4 Å/W-23.1 Å bilayers, with a total period of 40.5 Å, and it was grown

atop a standard oxidized silicon substrate wafer in the LBNL Center for X-ray Optics (CXRO). X-ray reflectivity measurements using Cu *K*α excitation verified the above numbers based on the initial synthesis parameters and also indicated that the B_4C/W interfaces interdiffused over about 3-4 Å. Previous standing wave [1] and TEM work has in addition shown that the top layer of the multilayer mirror expands by about 50% due to reaction with C and O in air [5], with all of these properties of the multilayer being included in the subsequent XRO modeling. The sample was grown on this multilayer at IBM Almaden Research Center as a Cr wedge of thickness ranging from 120-280 Å over a distance of 6 mm (thus spanning about 4 multilayer periods), a 16.2 Å Fe layer and an Al_2O_3 capping layer of 13.0 Å; the accuracies in these thicknesses are estimated to be ~2-3 Å.

The measurements were carried out at the variable-polarization undulator beamline 4.0.2 of the Berkeley Advanced Light Source (ALS) using the multi-technique spectrometer/diffractometer located there [6], which has recently been equipped with a Scienta XES 300 soft x-ray spectrometer. Samples were inserted via a loadlock and the base pressure in the main analysis chamber was 1.5 x 10^{-10} Torr. The Fe layer was magnetized using a 500 Oe field from an *in situ* electromagnet along the in-plane y direction indicated in Fig. 1. The magnetization was verified by measuring total-electron-yield x-ray magnetic circular dichroism (XMCD) for the Fe 2p levels, as shown in Fig. 2.

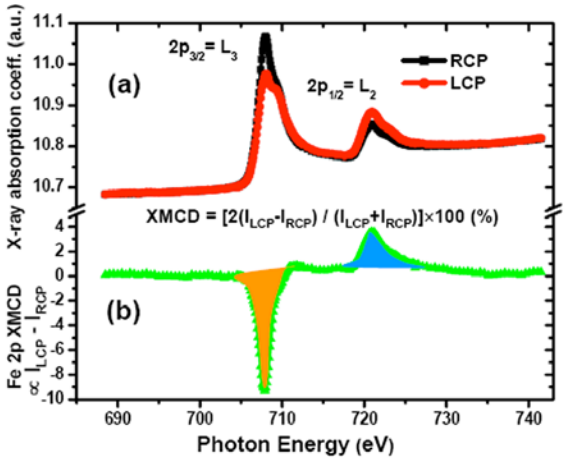

Fig. 2 – X-ray magnetic circular dichroism of the Fe 2p region obtained by total electron yield detection: (a) The individual intensities of left and right circularly polarized (LCP and RCP) light, as well as (b) the XMCD curve derived from them. The weakness of high-energy satellites in the spectra in (a) suggests a low degree of Fe oxidation.

The general form and magnitudes here are in good agreement with prior studies of Fe, as for example, in the work of Duda et al. on XMCD in XES and RIXS [7]. The experimental geometry was such that the incidence angle θ_{inc} was 12.9° and as near to the Bragg angle as could be estimated (see discussion below), and the emission angle θ_{em} was 48°.

Two types of experimental scans were performed, as done in the first swedge studies [1,2]. The first is a rocking curve performed at a fixed x position (and thus fixed wedge thickness) and variable incidence angle by rotating the sample relative to the light beam. The second is

done by fixing the angle at the first-order Bragg angle, as derived from an analysis of the rocking curve data and XRO calculations, and then scanning the sample along the x direction in Fig. 1 so as to vary the wedge thickness and effectively move the standing wave through the interfaces of interest. Since the standing wave is expected to have a period of 40.5 Å, the variation of the Cr wedge thickness over 160 Å means that we should in principle have been able to see up to four full periods of the standing wave as the sample was scanned along x.

All spectra shown here were taken with the exciting photon energy on the Fe L_2 resonance at ~721.5 eV (cf. Fig. 2), which yields via a detailed x-ray optical calculation using Kramers-Kronig analysis for calculating the precise optical constants in the Fe layer, a Bragg angle of 12.9°. Small discrepancies of such numbers from a standard Bragg's Law calculation for this multilayer of period 40.5 Å of 12.3º are due to refraction and phase shifts in the waves reflected and refracted at each of the interfaces due to small deviations from unity of the complex optical constants in each layer [8]. Broad x-ray emission spectra were recorded, as shown in Fig. 3, in order to monitor both the Fe $L_{\alpha,\beta}$ and Cr $L_{\alpha,\beta}$ intensities, as well as the resonant elastic scattering (REXS) peak at 721.5 eV, which strongly overlaps the Fe L_β emission peak that we find to be at ~720.0 eV. By measuring broad scan XES spectra for non-resonant excitation of Fe at 825 eV (data not shown here), we have determined that, for all spectra evaluated here, the presence of the elastic peak in the Fe $L_{\alpha,\beta}$ emission calls for an approximate 40% reduction in the total intensity measured over the Fe $L_{\alpha,\beta}$ + elastic region in order to describe only the $L_{\alpha,\beta}$ that is calculated in our XRO program in resonant excitation. Otherwise, the calculated relative intensities from the XRO program are not modified in our comparisons below with experiment.

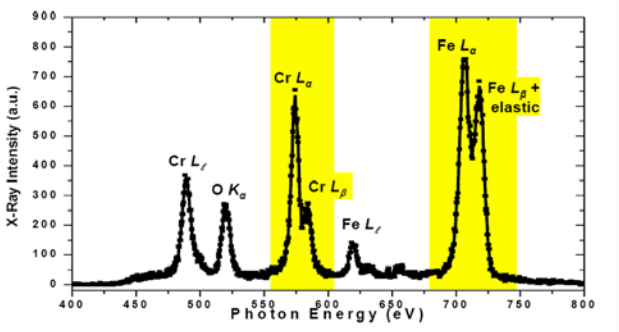

Fig. 3 – A typical broadscan XES/RIXS spectrum taken with an x position corresponding to a 220 Å thickness of the Cr wedge. LCP radiation at 721.5 eV was used for excitation. The Fe $L_{\alpha\beta}$ and Cr $L_{\alpha\beta}$ features of principle interest are highlighted.

Fig. 4 shows a rocking curve for the Cr $L_{\alpha,\beta}$/Fe $L_{\alpha,\beta}$ intensity ratio (with spectral intensity reduced by 40% to subtract off the elastic intensity), and is taken at an x position corresponding to a Cr thickness of 220 Å. All plots here are consistently displayed with a B-spline fit through the data. This data has been compared to a large family of x-ray optical calculations for various layer thicknesses and

wedge slopes around expected values based on the well-calibrated deposition conditions. Within the statistical accuracy of the experimental data, the agreement with theory is excellent, both as to the form and the magnitude of the curve. The behavior of this intensity-ratio rocking curve also provides us with the location of the Bragg angle (12.9°, and accurate estimates of the Fe and Cr layer thicknesses (16.2 Å and constant, and 220 Å for this choice of x, respectively).

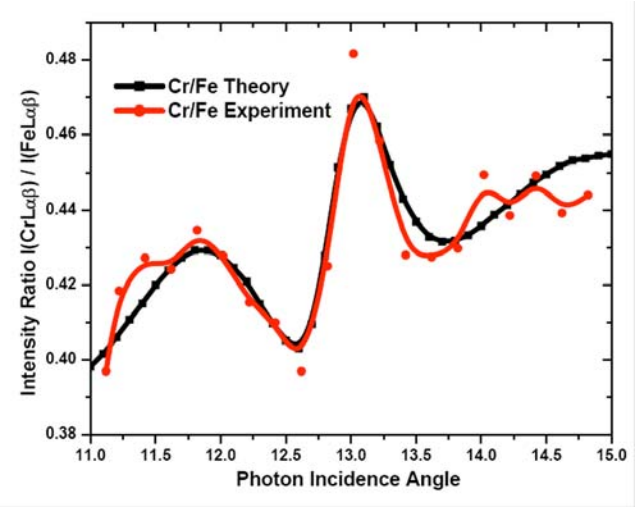

Fig. 4 – The Cr $L_{\alpha\beta}$/Fe $L_{\alpha\beta}$ intensity ratio as derived via a rocking curve scan over the Bragg angle at a Cr thickness of 220 Å. Both experiment and a best-fit XRO calculation are shown.

Tuning the sample to the position of the Bragg angle yields the largest modulation of the electric field through the sample, and this is then the angle at which the scan along the x direction is performed. As Fig. 1 illustrates, when the sample is scanned in this way, the incident beam moves along the wedge, with x-ray optical calculations confirming that the standing wave is pinned to the period of the multilayer mirror [1]. Thus, moving to positions along the wedge effectively moves the standing wave through the interface, modulating the intensities of the respective layers and interfaces according to their depths below the surface. This is the essence of the swedge method.

The intensities of the Fe $L_{\alpha,\beta}$, again adjusted to eliminate the elastic contribution, and Cr $L_{\alpha,\beta}$ are shown in Fig. 5 as a function of x position, which has now been converted to Cr thickness. Each spectrum has been systematically fit with Voigt functions and a linear background to determine the overall intensity. Since the Fe thickness is less than half of a period, the modulations are very strong while those of the Cr are much weaker since the thickness of the layer contains several standing wave periods (from three to seven over the wedge) and the emitted x-ray has a large attenuation length at 720 eV in the Cr of about 180 Å or four standing wave periods for our incidence angle. The modulations in intensity of both the Fe and Cr intensities are accurately described by the XRO calculations and, together with an analysis of the intensity ratio shown in Fig. 5(c) allow a more accurate determination of the Cr thickness over the full sample extent in x. The overall slope of the Cr intensity in Fig. 5(b) is due to the wedge form of the Cr layer, such

that as the wedge gets thicker, the Cr intensity goes up due to the high excitation and escape depths of the soft x-rays involved. The thin Fe layer on the other hand shows a simple damped sinousoidal form, with the damping due to the enhanced attenuation of the incident and reflected radiation as the Cr layer thickness increases.

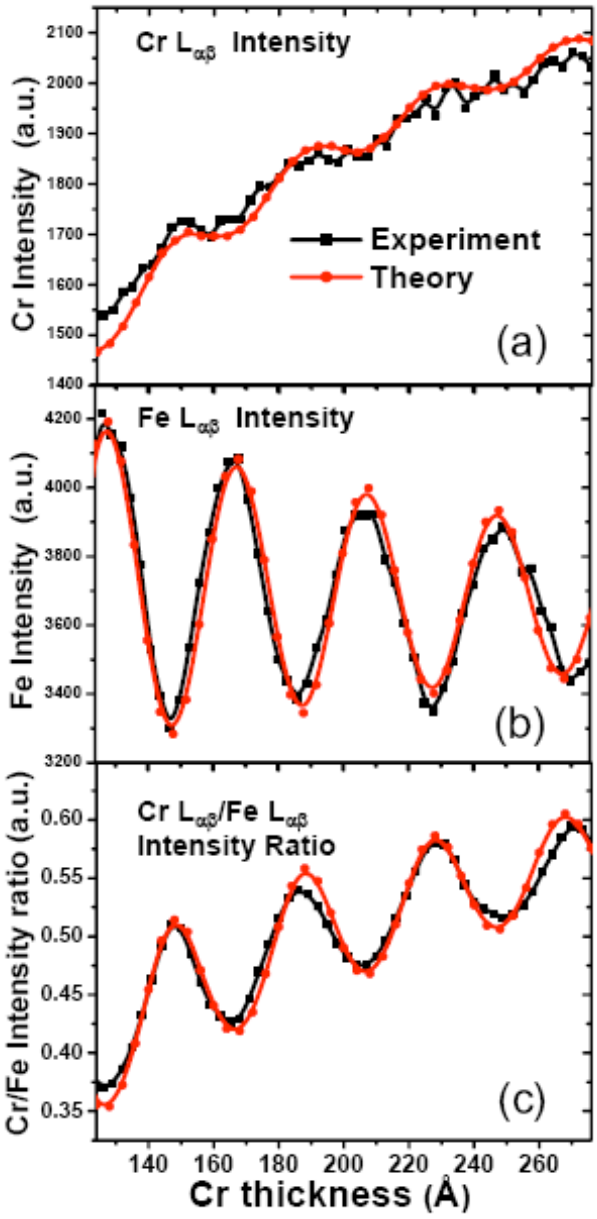

Fig. 5 – (a),(b) The individual Cr $L_{\alpha\beta}$ and Fe $L_{\alpha\beta}$ intensities (as summed over LCP and RCP), as well as (c) the ratio of these intensities, Cr $L_{\alpha\beta}$/Fe $L_{\alpha\beta}$, as derived by a standing-wave scan with sample motion along x and θ_{inc} fixed at the Bragg angle of 12.9°. The x position has been converted to Cr wedge thickness intensities as a function of Cr thickness at the Bragg angle.

In order to now determine the buried layer and interface properties in more detail, we focus on the overall form and the relative phases of both the RIXS total intensities and the Fe magnetic circular dichroism (MCD) results. We chose the Fe L_2 resonance energy for excitation, since it exhibits the strongest MCD effects in RIXS, as shown previously by Duda *et al.* [7]. Fig. 6 shows a typical set of x-ray emission dichroism results taken at a Cr thickness of 220 Å, in fact the same x position as the XAS spectra in Fig. 2, and Fig. 7 the various quantities observed as the sample is scanned in x. The MCD curve in Fig. 7(c) was determined from the formula

$$MCD = \frac{I(\mathrm{LCP}) - I(\mathrm{RCP})}{[\,I(\mathrm{LCP}) + I(\mathrm{RCP})]\,/\,2}, \qquad (1)$$

where the intensities are determined by peak-fitting with linear background subtraction. The relative dichroism magnitudes of both our XAS data in Fig. 2 and the RIXS data in Fig. 6 are again consistent with previous work by Duda *et al* [7]. There are also clear oscillations in the resulting MCD curves shown in Fig. 7, with overall amplitudes relative to the average of from 10% for smaller Cr thicknesses to 12% for larger

thicknesses. The form of the MCD curve is different, however, from those in Figs. 7(a) and 7(b) used to derive it, in that the peaks are broader and somewhat flat-topped, with minima that are distinctly sharper, even after allowing for the greater statistical uncertainty in the ratio of Eq. 1. There is also a reproducible left-right

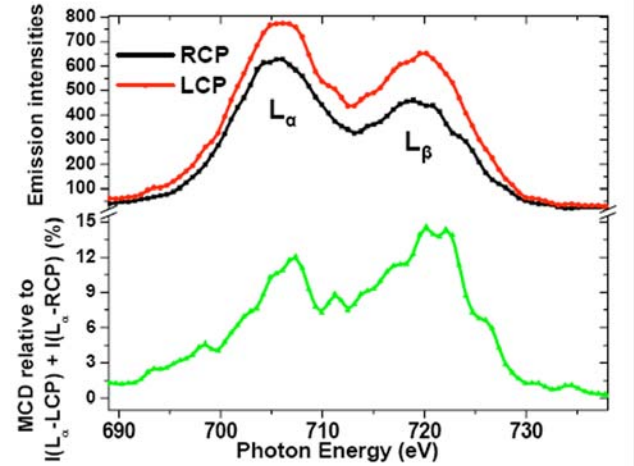

Fig. 6 – Fe $L_{\alpha\beta}$ x-ray RIXS magnetic circular dichroism taken at 220 Å Cr thickness and an excitation energy of 721.5 eV at the L_2 absorption resonance. Dichroism is plotted as a percentage of the L_α peak heights.

asymmetry within each peak, with the intensity at smaller Cr thicknesses being higher. There is finally a phase shift between the total Fe intensity and the centroids of the MCD peaks of approximately 3-4 Å, with the MCD being at slightly larger Cr thickness, as can be seen visually, but also has been derived by least-squares fitting sinusoidal functions to both the intensity and MCD data [9]. Finally, as we demonstrate more precisely below via the detailed mathematical modeling of intensity and MCD in such a swedge scan, the fact that any non-zero MCD modulations are observed in Fig. 7(c) implies that the contribution of Fe per atom

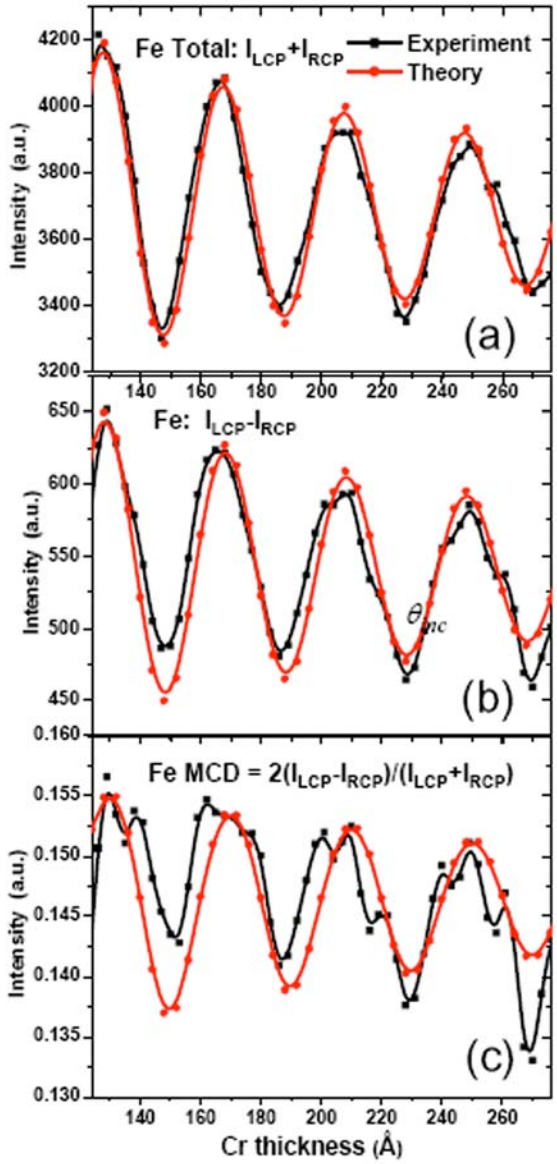

Fig. 7 – Standing-wave scans in x (or Cr thickness) of Fe $L_{\alpha\beta}$ x-ray emission magnetic circular dichroism: (a) total Fe intensity as measured by I_{LCP} + I_{RCP}, (b) the quantity I_{LCP} - I_{RCP} that is proportional to Fe magnetization, and (c) the final Fe MCD as defined in the text.

to dichroism is not constant for all Fe atoms, but rather decays through the interfaces to both Cr on the bottom and Al_2O_3 on the top.

In order to more quantitatively analyze this data, we now introduce some basic phenomenological equations describing x-ray intensity as excited by right and left circular polarization:

$$I_{\mathrm{RCP}}(\theta_{inc},x) = C\int[1+\mu_{\mathrm{RCP}}(z)]\,|\vec{E}_{\mathrm{SW}}(\theta_{inc},x,z)|^2 e^{-z/\Lambda_x\sin\theta_{em}}\rho(z)\frac{d\sigma_x}{d\Omega}dz$$
$$I_{\mathrm{LCP}}(\theta_{inc},x) = C\int[1+\mu_{\mathrm{LCP}}(z)]\,|\vec{E}_{\mathrm{SW}}(\theta_{inc},x,z)|^2 e^{-z/\Lambda_x\sin\theta_{em}}\rho(z)\frac{d\sigma_x}{d\Omega}dz \quad (2),$$

where C is a constant, $\mu_{\mathrm{RCP}}(z)$ and $\mu_{\mathrm{LCP}}(z)$ are the depth-dependent contributions of a given atomic type to the magnetic dichroism, $|\vec{E}_{\mathrm{SW}}(\theta_{inc},x,z)|^2$ is the electric field strength squared of the standing wave for a given incidence angle and at a given depth z as is calculated in our XRO program, $e^{-z/\Lambda_x\sin\theta_{em}}$ represents the attenuation of the outgoing x-ray due to absorption, $\rho(z)$ is the atomic density at a given depth, and $\frac{d\sigma_x}{d\Omega}$ is the differential cross section for x-ray emission or scattering in a given line. The dependence on incidence angle included here implies that these expressions will also apply to rocking curve measurements. We further note that $\mu_{\mathrm{RCP}}(z)$ and $\mu_{\mathrm{LCP}}(z)$ can be written as proportionalities of the form $\mu_{\mathrm{RCP}}(z) = \hat{e}_{\mathrm{RCP}}m(z)$ and $\mu_{\mathrm{LCP}}(z) = \hat{e}_{\mathrm{LCP}}m(z)$, where $\hat{e}_{\mathrm{RCP}}$ and $\hat{e}_{\mathrm{LCP}}$ are constants and $m(z)$ is the depth-dependent magnetization per atom due to a specific atomic type, here of course Fe.

Now following Eq. 1 by taking the difference of these two intensities and dividing by their average yields the magnetic circular dichroism:

$$I_{\mathrm{MCD}}(\theta_{inc},x) = \frac{\left[\int[1+\mu_{\mathrm{LCP}}(z)]\,|\vec{E}_{\mathrm{SW}}(\theta_{inc},x,z)|^2 e^{-z/\Lambda_{em}\sin\theta_{em}}\rho(z)\frac{d\sigma_x}{d\Omega}dz - \int[1+\mu_{\mathrm{RCP}}(z)]\,|\vec{E}_{\mathrm{SW}}(\theta_{inc},x,z)|^2 e^{-z/\Lambda_{em}\sin\theta_{em}}\rho(z)\frac{d\sigma_x}{d\Omega}dz\right]}{\left[\int[1+\mu_{\mathrm{LCP}}(z)]\,|\vec{E}_{\mathrm{SW}}(\theta_{inc},x,z)|^2 e^{-z/\Lambda_{em}\sin\theta_{em}}\rho(z)\frac{d\sigma_x}{d\Omega}dz + \int[1+\mu_{\mathrm{RCP}}(z)]\,|\vec{E}_{\mathrm{SW}}(\theta_{inc},x,z)|^2 e^{-z/\Lambda_{em}\sin\theta_{em}}\rho(z)\frac{d\sigma_x}{d\Omega}dz\right]/2} \quad (3).$$

We now note that, if the contribution of each atom of this type to magnetic dichroism is the same, regardless of its position inside a given layer or in an interface between two layers, it is equivalent to both μ_{RCP} and μ_{LCP} being independent of z, in which case we have

$$I_{\mathrm{MCD}}(\theta_{inc},x) = \frac{2[\mu_{\mathrm{LCP}}-\mu_{\mathrm{RCP}}]\int|\vec{E}_{\mathrm{SW}}(\theta_{inc},x,z)|^2 e^{-z/\Lambda_x\sin\theta_{em}}\rho(z)\frac{d\sigma_x}{d\Omega}dz}{[2+\mu_{\mathrm{LCP}}+\mu_{\mathrm{RCP}}]\int|\vec{E}_{\mathrm{SW}}(\theta_{inc},x,z)|^2 e^{-z/\Lambda_x\sin\theta_{em}}\rho(z)\frac{d\sigma_x}{d\Omega}dz} = \frac{2[\mu_{\mathrm{LCP}}-\mu_{\mathrm{RCP}}]}{2+\mu_{\mathrm{LCP}}+\mu_{\mathrm{RCP}}} \approx \mu_{\mathrm{LCP}}-\mu_{\mathrm{RCP}} \quad (4),$$

where the last approximate equality holds if both μ_{RCP} and μ_{LCP} are much less than unity. Eq. 4 thus implies that the MCD will be constant during a standing wave scan in z or in fact also a rocking curve scan in θ_{inc}, unless the

contributions of a given atom to dichroism as a function of depth differ from the concentration profile of that atom. An alternative, and very useful, way of looking at this is that, if the MCD is found to vary during a standing wave scan or rocking curve measurement, the contribution of a given atom to dichroism is not constant through the layer or through one or both of the interfaces bounding the layer containing that atom.

From this discussion of Eqs. (3) and (4) and the results of Fig. 7(c), it is clear that the atom-specific iron contributions to magnetization are not constant through the Fe interfaces. The XRO calculations we have carried out to analyze these data more quantitatively begin by defining the thicknesses t_i of each of the layers involved, where i = Al_2O_3, Fe, Cr, B_4C(expanded top), W, B_4C(ML), including all layers within the multilayer. These are initially set to values t^0_i given by the synthetic recipe and, for the ML, the values derived from the hard x-ray reflectivity measurements. In describing the interfaces between all layers in the sample and the multilayer substrate, the program further assumes concentration and refractive index gradients with linear profiles characterized by basewidths w_{ij}, where ij refers to the upper or lower layers involved. Setting these widths to zero corresponds to no interface roughness or interdiffusion. Conservation of mass is also required, such that the total amount of each atom is kept constant as the interface width is varied; that is, for a given layer, t_i must decrease from t^0_i as the widths $w_{i,upper}$ and/or $w_{i,lower}$ are increased from zero. More quantitatively, $t^0_i = w_{i,upper}/2 + t_i + w_{i,lower}/2$. Beyond this, for any magnetic atoms in the sample, with Fe being the only case

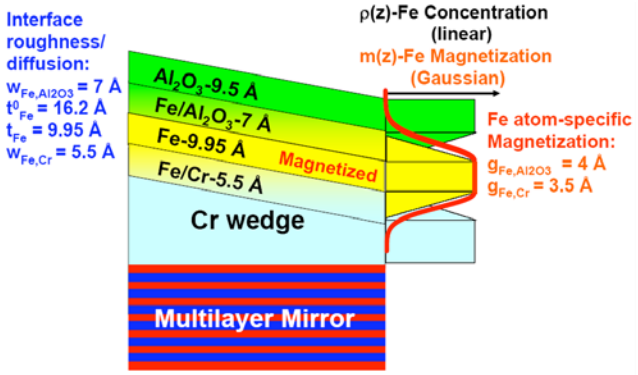

Fig. 8 – Top and bottom interface structures as derived by best fits of x-ray optical calculations to the data in Figs. 4, 5, and 7. Interface concentration profiles are assumed to be linear. Atom-specific magnetization profiles are assumed to be Gaussian. The best-fit parameters are also indicated. The functional form of the concentration and the magnetization are shown, with each function normalized to the value in the center of the Fe layer in which there is no interdiffusion/roughness and the magnetization is constant.

considered here as the Cr MCD was too weak to measure accurately, the variation of the atom-specific contribution to magnetization m(z) through all interfaces is assumed to decay away from a constant-magnetization ferromagnetic layer of thickness t_i via a Gaussian profile with a half-width at half-maximum value of

$g_{ij} = \sqrt{2\ln 2}\sigma_{ij} \approx 1.177\sigma_{ij}$. The form of these variations is illustrated in Fig. 8.

The XRO calculations shown in Fig. 7 represent an optimized fit to this Fe data over many trial choices of all five parameters related to it: $t_{Fe,}$ $w_{Fe,Al2O3}$, $g_{Fe,Al2O3}$, $w_{Fe,Cr}$ and $g_{Fe,Cr}$. The final theoretical curves correspond to the parameters given in Fig. 8*:* t_{Fe} = 9.95 Å, $w_{Fe,Al2O3}$ = 7 Å, $g_{Fe,Al2O3}$ = 4.0 Å, $w_{Fe,Cr}$ = 5.5 Å and $g_{Fe,Cr}$ = 3.5 Å. Since the initial total Fe thickness as deposited was 16.2 Å, these values are atom-conserving, since 7/2 + 9.95 + 5.5/2 = 16.2. XRO theory with these parameters fits both the total intensity and LCP-RCP curves in Figs. 7(a) and 7(b) very well. The MCD data in Fig. 7(c) is reasonably well described, including the phase shift to larger Cr thicknesses, although with bigger differences between experiment and theory in that theory yields somewhat more symmetric and sinusoidal peaks than experiment. However, the noise level in the MCD results makes it difficult to conclude that this is a serious problem with our simulation.

We have also confirmed via much simpler model calculations in which $|\vec{E}_{SW}(\theta_{inc}, x, z)|^2$ is simply assumed to be a sinusoidal function and x-ray attenuation is neglected in Eqs. 2 and 3 that the MCD curve should exhibit both a phase shift and an asymmetry of the type observed experimentally if the top and bottom interfaces of a layer are not identical.

In order to explore the sensitivity of the analysis of our MCD data via Eqs. 2 and 3 with no simplifications to the choice of parameters, we now show in Fig. 9 curves for several choices as systematically varied around our optimum values. In Fig. 9(a), we show what happens when only the Fe/Cr interface thickness is systematically increased in steps from the limiting case where both $w_{Fe,Cr}$ and $g_{Fe,Cr}$ are zero (a sharp interface) to our optimum value, and then increasing beyond this, but keeping the ratio $g_{Fe,Cr}$ /$w_{Fe,Cr}$ constant, and in Fig. 9(b) a similar series in which only the Fe/Al_2O_3 interface thickness is increased via $w_{Fe,Al2O3}$ and $g_{Fe,Al2O3}$ in the same way. From these calculations, we can see that our choice of parameters for both interfaces best predict the phase shift in the MCD with respect to the total intensity, and that this phase shift quickly diverges from the experimental data if we move away from this choice. We thus conclude that the accuracy in our choice of the parameters $w_{Fe,Al2O3}$, $g_{Fe,Al2O3}$, $w_{Fe,Cr}$ and $g_{Fe,Cr}$ is approximately ±3 Å, and thus is similar to the accuracy found in the first swedge study of the Fe/Cr interface using photoemission [1].

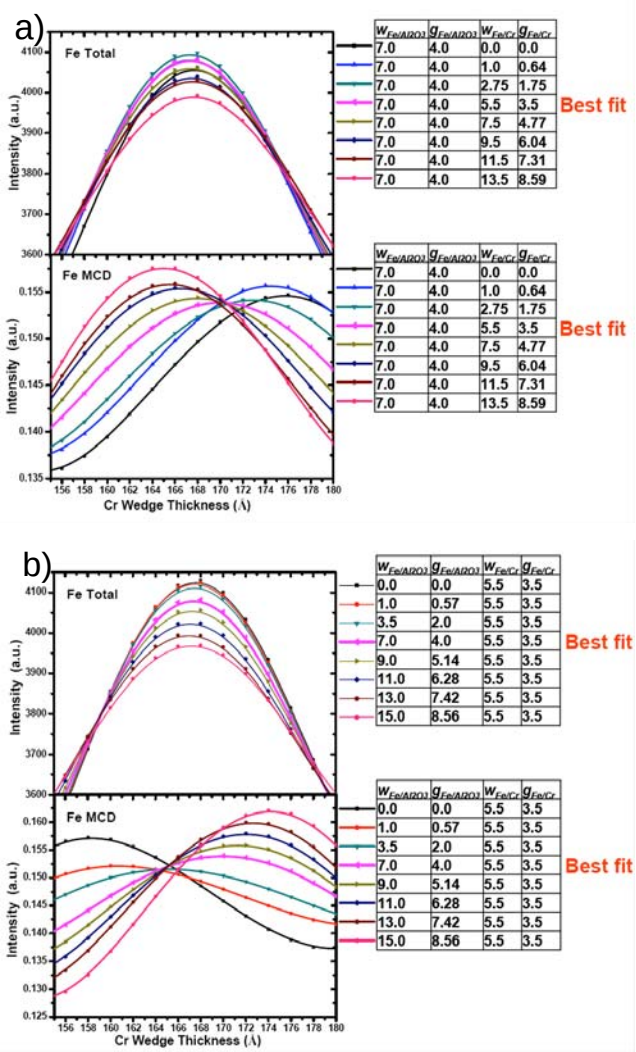

Fig. 9 – X-ray optical calculations of Fe total intensity and RIXS MCD in which parameters have been systematically varied around the optimum fit to the experimental data: (a) only the thickness of the Fe/Cr interface is varied, with the ratio $g_{Fe/Cr}/w_{FeCr}$ also constant, (b) only the thickness of the Fe/Al_2O_3 interface is varied, with the ratio $g_{Fe/Al2O3}/w_{Fe/Al2O3}$ also constant. All parameters are given in Angstroms.

As one final assessment of error limits, in Fig. 10 we show additional calculations in which various combinations of concentration and magnetization interface widths are chosen, including our optimum as compared directly to experiment again, but also first varying both w and g upward on one interface by 50% (i.e. multiplying by 1.5x) and downward on the other interface simultaneously by 50% (i.e. multiplying a factor of 0.5). The curves for these choices clearly do not fit experiment as well, and are qualitatively consistent with the error limits estimated above.

Beyond these calculations, Fig. 10 also shows what happens in the numerical calculation if the Gaussian width associated with the atomic contribution to magnetization is made extremely large on both interfaces. In this case, all atoms in the interface contribute equally to magnetization, and this is equivalent to μ_{RCP} and μ_{LCP} being independent of z. The numerical calculation for this case in fact yields a constant dichroism, as expected from Eq. (4). In addition, these curves show that, if the interface becomes sharp in both concentration and magnetization, there is still no dependence on z so the MCD is again a constant. As intermediate cases, as we more subtly increase the Gaussian widths of the magnetic contribution around the Fe, such as shown for the 25Å and 50Å choices for *g*, the modulations of the calculated MCD systematically decrease and the curves approach unity.

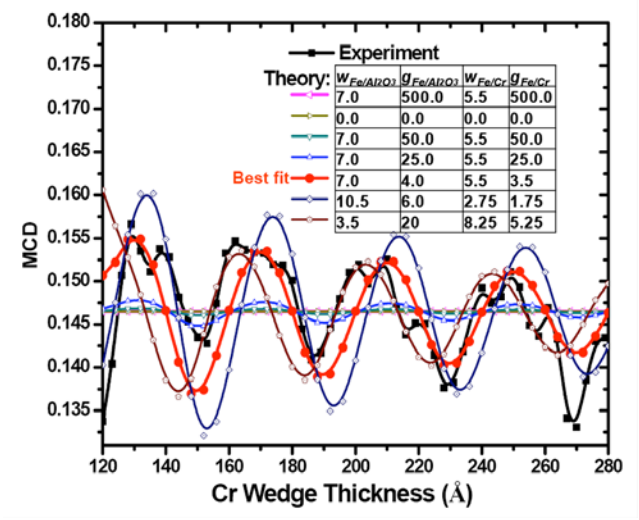

$w_{Fe/Al2O3}$	$g_{Fe/Al2O3}$	$w_{Fe/Cr}$	$g_{Fe/Cr}$
7.0	500.0	5.5	500.0
0.0	0.0	0.0	0.0
7.0	50.0	5.5	50.0
7.0	25.0	5.5	25.0
7.0	4.0	5.5	3.5
10.5	6.0	2.75	1.75
3.5	20	8.25	5.25

Fig. 10 – X-ray emission MCD measurements as a function of Cr thickness are compared with theoretical calculations for various choices of parameters, including the best fit as well as several other calculations used to illustrate the sensitivity of the fits. The calculations include upward and downward variations in the thickness of the top and bottom interfaces, as well as extreme limits in which the atom-specific magnetization is constant through both interfaces (e.g. with $g_{Fe/Al2O3}$ and $g_{Fe/Cr}$ = 500 Å) and the MCD becomes constant in the standing-wave scan.

Finally, we note that the numbers at which we have arrived for the Fe/Cr interface of $w_{Fe,Cr}$ = 5.5 Å and $g_{Fe,Cr}$ = 3.5 Å through this x-ray emission study are in fact very close to a set of numbers derived through another swedge study using photoelectron emission: $w_{Fe,Cr}$ = 6.8 Å and $g_{Fe,Cr}$ = 2.8 Å [1]. But a key difference in the present work is being able to look at both the top and bottom interfaces of Fe, even in the presence of the alumina capping layer, due to the greater escape depths of the x-rays. In fact, in this earlier study, no capping layer was used to avoid excessive attenuation of the Fe photoelectron intensities, with both the Fe and Cr layers being grown *in situ*.

In conclusion, we have demonstrated that the standing wave/wedge (swedge) method can be used with soft x-ray emission and resonant inelastic x-ray scattering to non-destructively determine concentration and atom-specific magnetization profiles in a multilayer nanostructure. These properties have been determined for both the upper and lower interfaces of Fe sandwiched between capping alumina and Cr. Using the swedge method with x-ray emission/scattering thus greatly expands the range of buried interfaces and sample types that can be accurately and quantitatively profiled.

This work was supported by the Director, Office of Science, Office of Basic Energy Sciences, Materials Science and Engineering Division, U.S. Department of Energy under Contract No. DE-AC03-76SF00098.

References

[1] S.-H. Yang, B.S. Mun, N. Mannella, S.-K. Kim, J.B. Kortright, J.H. Underwood, F. Salmassi, E. Arenholz, A. Young, Z. Hussain, M.A. Van Hove, C.S. Fadley, J. Phys.: Condens. Matter **14** (2002) L407-L420.

[2] S.-H. Yang, B.S. Mun, N. Mannella, A. Nambu, B.C. Sell, S.B. Ritchey, F. Salmassi,

A. Shick, S.S.P. Parkin, C.S. Fadley, J. Phys.: Condens. Matter **18** (2006) L259–L267

[3] S.-H. Yang, Computer program to predict photoelectron or x-ray emission intensities including all x-ray optical excitation and electron or x-ray escape processes, to be published.

[4] L.T. Kuhn A. Bojesen, L. Timmermann, K. Fauth, E. Goering, E. Johnson, M.M. Nielson, S. Morup, J. Magn. and Magn. Mater. **272-276** (2004) 1485-1486

[5] S.-H. Yang, B.S. Mun A.W.Kay, S.-K. Kim, J.B. Kortright, J.H. Underwood, Z. Hussain, C.S. Fadley, J. Electron Spectrosc. Relat. Phenom. **114-116** (2001) 1089-1095.

[6] C.S. Fadley, M.A. Van Hove, Z. Hussain, A.P. Kaduwela, J. Electron Spectrosc. Relat. Phenom. **75** (1995) 273.

[7] L.-C. Duda, J. Stohr, D.C. Manicini, A. Nilsson, N. Wassdahl, J. Nordgren, and M.G. Samant, Phys. Rev. B, **50** (1994) 22.

[8] B.L. Henke, E.M. Gullikson, and J.C. Davis, *At. Data Nucl. Data Tables* **55** (1993) 34.

[9] B.C. Sell, Ph.D. Thesis, Department of Physics, University of California., Davis (2007).